JOURNAL OF SYNCHROTRON RADIATION

ISSN 1600-5775

Absorption and scattering by structured interfaces in X-rays

Leonid Goray*

Alferov University, 8/3 Let. A Khlopin St., St Petersburg 194021, Russia, ITMO University, 49 Kronverkskiy Pr., St Petersburg 197101, Russia, and Institute for Analytical Instrumentation of RAS, 26 Rizhsky Pr., St Petersburg 190103, Russia. *Correspondence e-mail: lig@pcgrate.com

Received 31 July 2020
Accepted 29 October 2020

Edited by Y. Amemiya, University of Tokyo, Japan

Keywords: absorption; scattering intensity; X-rays; diffraction grating; rough mirror.

Promising achievements of resonance inelastic X-ray scattering and other spectroscopy studies in the range from hard X-ray to extreme ultraviolet require the development of exact tools for modeling energy characteristics of state-of-the-art optical instruments for bright coherent X-ray sources, space science, and plasma and superconductor physics. Accurate computations of the absorption and scattering intensity by structured interfaces in short wavelength ranges, *i.e.* realistic gratings, zone plates and mirrors, including multilayer-coated, are not widely explored by the existing methods and codes, due to some limitations connected, primarily, with solving difficult problems at very small wavelength-to-period (or to correlation length) ratios and accounting for random roughness statistics. In this work, absorption integrals and scattering factors are derived from a rigorous solution of the vector Helmholtz equations based on the boundary integral equations and the Monte Carlo method. Then, using explicit formulae (in quadratures), the author finds the absorption and scattering intensity of one- and bi-periodic gratings and mirrors, which may have random roughnesses. Examples of space and spectral power distributions for gratings and mirrors working in X-rays are compared with those derived using the usual indirect approach and well known approximations.

1. Introduction

An accurate and fast computing of the absorption magnitude A (*i.e.* resistive dissipation of electromagnetic wave energy called Joule's heat and normalized to the incidence radiation energy) in structured layers is very important for many applications. For gratings, examples are: microwave (Sisodia & Gupta, 2007) and optical (Loewen & Popov, 1997; Rathsfeld *et al.*, 2006) devices, for lithography processes (Smith & Suzuki, 2007), in solar cell improvements (Nanotechnology, 2014); and also such modern fields as plasmonics (Enoch & Bonod, 2012) and metamaterials (Liu & Zhang, 2011), where absorption plays a predominant role. For optics and optical instruments working in the tender-X-ray–extreme ultraviolet (EUV) range, values of A and also the scattering intensity η are most relevant (Goray & Schmidt, 2010; Goray, 2010*a*) due to a lot of critical applications in such fields as resonance inelastic X-ray scattering (RIXS) (Strocov *et al.*, 2010; Ament *et al.*, 2011; Voronov *et al.*, 2016; Goray & Egorov, 2016), X-ray free-electron lasers (XFELs) and synchrotron radiation sources of the fourth generation (Choueikani *et al.*, 2014; Yashchuk *et al.*, 2015; Vannoni & Freijo-Martin, 2017; Huang *et al.*, 2017; Goray *et al.*, 2018; Siewert *et al.*, 2018), X-ray microscopy (Jacobsen *et al.*, 2019), soft-X-ray–EUV lithography (Goray, 2007; Chkhalo & Salashchenko, 2013; Bakshi, 2018) and space and laboratory spectroscopy of plasma physics (Seely *et al.*, 2011; Marlowe *et al.*, 2016; Marshall *et al.*, 2018; Shatokhin *et*

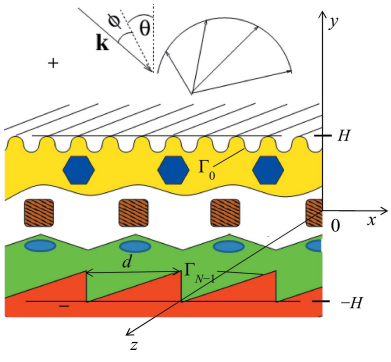

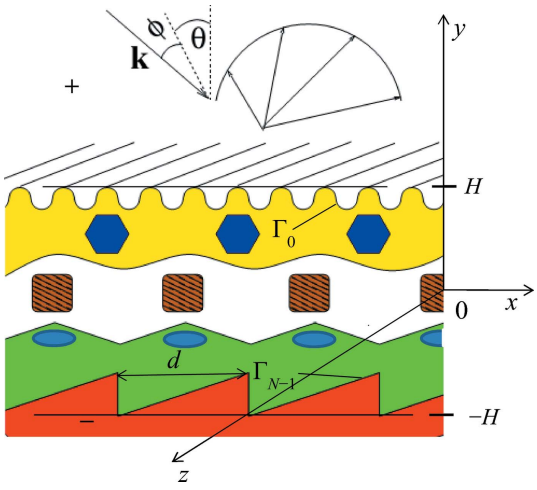

Figure 1
Schematic conical diffraction by a multilayer one-periodic grating.

al., 2018; Lingam & Loeb, 2020), *etc*. Because of the transverse electric (TE) (polarization wherein the electric field is perpendicular to the plane of incidence) and transverse magnetic (TM) (polarization wherein the electric field is in the plane of incidence) modes in cases for one-periodic (classical) gratings working in conical diffraction (Goray & Schmidt, 2012) (see Fig. 1) or bi-periodic (crossed) gratings (bi-gratings, Fig. 2) being coupled through the boundary conditions, the associated 3D diffraction problems are more general, and gratings, including multilayer-coated, can act as volume- and surface-field enhancers or absorbers at any incidence polarization state. In various disordered or random nanostructures similar type properties can occur (Weitz *et al.*, 1980; Maystre & Saillard, 1994; Stuart & Hall, 1998; Stockman *et al.*, 2001; Nau *et al.*, 2007). Besides being physically meaningful, a computation of A, as well as using the reciprocity theorem (Petit, 1980), is an important tool to check the quality of the numerical solution for absorbing gratings, Fresnel zone plates and rough mirrors with the requirement that the sum of reflected, transmitted and total absorbed energies (powers, for stationary processes) should be equal to the energy of the incident wave. In some cases, direct calculus of A using Poynting's vector gives divergent or non-correct results;

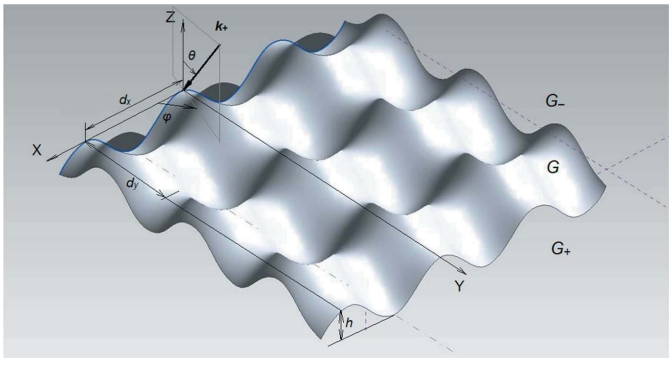

Figure 2
Schematic diffraction by a bi-periodic grating.

'however, when the definition has been applied cautiously, in particular for averages over small but finite regions of space or time, no contradictions with experiments have been found' (Born & Wolf, 2002).

The motivation for the present work is a derivation on the basis of the known analytically proved approaches and applying general expressions for calculation of A and η of one-periodic and bi-periodic X-ray gratings and general randomly rough structures in the closed form, namely as surface integrals versus electromagnetic field solutions. It is worth noting that a computation of A itself is not connected with the specific wavelength range and rigorous method, which are used for near-zone electromagnetic field calculus. Such a computation has not only intuitive significance but the same rigor, namely in the sense of distributions (generalized functions). Moreover, the derivation of the generalized energy balance for absorption gratings is similar to a deduction of the classical energy conservation laws for perfectly conducting and lossless gratings (see, for example, Popov, 2014, ch. 2). In the electromagnetic literature there are various expressions for absorption calculus in particular cases, however without a derivation of general formulae and references to mathematical results for diffraction gratings. Botten *et al.* (1981) considered the absorption of lamellar one-periodic gratings for in-plane (classical) diffraction and TE/TM polarizations using the modal method. Budzinski *et al.* (1991) gave the local dissipation density in the metal of a sinusoidal grating profile inside and outside an anomaly in explicit form. Jarem & Banerjee (1999) evaluated the general power balance for an anisotropic non-Hermitian one-periodic grating for the TM polarization using the rigorous coupled-wave analysis. Botten *et al.* (2000) presented the energy conservation properties for wave propagation through stacked gratings comprising metallic and dielectric cylinders using the Green's function approach based on lattice sums to obtain the scattering matrices of each layer. Roger *et al.* (1984) established the energy-balance criterion described for nonlinear in-plane one-periodic and rough surfaces in the explicit form for both basic polarization states and derived from Maxwell's equations. Popov (2014, ch. 12) derived the generalized energy balance in the explicit form for multilayer-coated isotropic one-periodic gratings working in classical and conical diffraction from the boundary integral equation theory using the absorption integrals. Petit (1980, ch. 7) obtained the energy absorption formula for isotropic bi-gratings using the coordinate transformation technique and boundary integral equations. And Popov (2014, ch. 5) presented the global energy balance for inhomogeneous anisotropic one- and bi-gratings using the finite-element method and variational formulation of the diffraction problem.

There are two classical and equivalent approaches in electromagnetism, with some restrictions in each of them, to model light scattering intensities (effective radar cross sections) for rough surfaces. The most general and time-consuming one is using large surface lengths of many wavelengths λ. In this approach some window functions and tapered (narrowing) beams can be used to restrict the illu-

minated range and avoid numerical difficulties at endpoints (Saillard & Maystre, 1988). The second widely explored approach is using periodic boundary conditions (quasi-periodicity of Floquet–Bloch modes). This method uses an infinite beam (plane wave) and assumes that the random rough surface length having some numbers of asperities repeats itself for given large periods (Nieto-Vesperinas & Dainty, 1990). That means using infinite grating samples and their periodicity together with intensive Monte Carlo simulations (Sadiku, 2009). In most electromagnetic methods to find scattering intensities, the Monte Carlo technique is employed to average deterministic scattered fields due to individual rough surfaces over a random ensemble of realizations. Scattered amplitudes are rigorously computed for each surface realization and, then, combined incoherently to obtain average scattering coefficients as an ergodic process. From theoretical and numerical reasons we thought it convenient to use the large-period grating model in the short-wavelength range.

The current approach is presented for the general case of inhomogeneous (multilayer-coated) randomly rough bi-gratings. Such an approach was partially presented in a couple of brief conference papers including some mathematics (Goray, 2015, 2016), however without any numerical examples and discussions. A case of one-periodic gratings will be described here briefly and addressed, mostly, to the references in the literature. However, the final formulae and numerical examples are presented and discussed. A presentation of explicit expressions considered for finding the absorption quantity, as well as the scattering coefficients obtained for various diffraction structure types, bear only on Maxwell's equations (or vector Helmholtz equations), the divergence (Gauss-Ostrogradsky) theorem and the rigorous boundary conditions. Besides more generality, the present formulation is based on the developed mathematical foundation (Dobson & Friedman, 1992; Dobson, 1994; Bao *et al.*, 1995; Bao, 1997; Bao & Dobson, 2000; Schmidt, 2003; Bugert & Schmidt, 2015) and related publications via variational (weak) and integral-equation formulations of one- and bi-periodic grating diffraction problems including the existence, uniqueness and convergence of the electromagnetic field solution. The variational and integral equation formulations has the great advantage that it is applicable to very general diffraction gratings with any topology of interfaces and materials: bi-periodic, inhomogeneous, anisotropic, negatively refracted, *etc*. Thus, the energy balance generalization and computation in the explicit form (in quadratures) of A and η for complex one- and bi-periodic gratings and rough mirrors can be considered as having both academic and practical importance. The paper is organized as follows. The diffraction problem for a general bi-grating is described in Section 2. A generalization of the energy balance, absorption and scattering intensity for bi-gratings, classical gratings and rough 2D surfaces is formulated in Section 3. Several numerical results devoted to various absorption or scattering problems, *i.e.* of the multilayer W/B_4C blaze grating working in classical and conical soft-X-ray diffraction, randomly rough multilayer Mo/Si lamellar grating working in the EUV, 1D rough GaAs surface investigating in hard X-rays and rough 2D Au surfaces working in soft X-rays, are presented in Section 4.

2. Diffraction problem

We consider the general case of vector diffraction by an arbitrary crossed grating with periods d_x and d_y directed, in general, non-orthogonally. Consider a time-harmonic [with time-dependence $\exp(-i\omega t)$] electromagnetic linearly polarized plane wave incident from above (+) on a bi-periodic lossy structure G bounded in $\mathbf{R}^3$ and separated by two homogeneous half-spaces $G_+ := \{z \geq 0\}$ and $G_- := \{z \leq -h\}, h \geq 0$, in Cartesian coordinates $(x, y, z) = \mathbf{r} \in \mathbf{R}^3$ (Fig. 2). We assume constant relative electric permittivity $\epsilon_\pm$ and constant relative magnetic permeability $\mu_\pm$ such that $\operatorname{Re}\epsilon_+ > 0 \wedge \operatorname{Re}\mu_+ > 0$, $\operatorname{Im}\epsilon_+ = 0 \wedge \operatorname{Im}\mu_+ = 0 \wedge \operatorname{Im}\epsilon_- \geq 0 \wedge \operatorname{Im}\mu_- \geq 0$ and $\epsilon_\pm \neq 0 \wedge \vee\ \mu_\pm \neq 0$. Otherwise, the relative permittivity $\hat{\epsilon}(x, y, z)$ and permeability $\hat{\mu}(x, y, z)$ functions of the grating region G are given by nonsingular 3×3 matrices with doubly periodic, complex-valued L^∞ (bounded) components. In physics, these components are usually piecewise continuous or piecewise constant functions corresponding to material refractive indices. Thus, we allow rather general anisotropic bi-periodic structures including edges, intersected surfaces, inclusions and also metamaterials.

It is important in the treatment of periodic problems that we restrict the consideration to one unit-cell $G := \{\mathbf{r} \in \Gamma \times \mathbf{R}: -h \leq z \leq 0\}$, for one biperiod $\Gamma := [0, d_x) \times [0, d_y)$ and uniform regions $G_\pm$ above and below G such that $G_+ := \{\mathbf{r} \in \Gamma \times \mathbf{R}: z > 0\}$ and $G_- := \{\mathbf{r} \in \Gamma \times \mathbf{R}: z < -h\}$ (thus, $\overline{G}$ is a compact set).

In the physical problem the surface is illuminated by an electromagnetic plane wave with the incident wavevector $\mathbf{k}_+ = (\alpha, \beta, -\gamma)^{\mathrm{T}}$,

$$u^i = (\mathbf{E}^i, \mathbf{H}^i) = (\mathbf{p}, \mathbf{s}) \exp[i(\alpha x + \beta y - \gamma z)]. \tag{1}$$

In (1), polarization vectors $\mathbf{p}$, $\mathbf{s}$ satisfy

$$\mathbf{k}_+ \cdot \mathbf{p} = \mathbf{k}_+ \cdot \mathbf{s} = \mathbf{s} \cdot \mathbf{p} = 0.$$

Due to the grating periodicity the incident wave is scattered into a finite number of plane waves in $G_+ \times \mathbf{R}$ and possibly in $G_- \times \mathbf{R}$. $|k_+| = k_v(\epsilon_+\mu_+)^{1/2}$, where $k_v = w/c$, ω is a fixed positive frequency and c is the vacuum light velocity. Note that this condition is satisfied by dielectric media with $\varepsilon_+ > 0$, $\mu_+ > 0$ as well as negative index materials, satisfying $\varepsilon_+ < 0$, $\mu_+ < 0$. The wavevector $\mathbf{k}_+$ is expressed using the incidence angles $|\theta| < \pi/2$, $|\phi| < 2\pi$ and the polarization angle $|\Psi| < \pi$: $\mathbf{k}_+ = k_v\nu_+(\sin\theta\cos\phi, \sin\theta\sin\phi, -\cos\theta)^T$ and $p_x = \cos\Psi\cos\theta\cos\phi - \sin\Psi\sin\phi$, $p_y = \cos\Psi\cos\theta\sin\phi + \sin\Psi\cos\phi$, $p_z = -\cos\Psi\sin\theta$. For the upper refractive index $\nu_+ = (\epsilon_+\mu_+)^{1/2}$ we determine $\gamma > 0$ if $\varepsilon_+ > 0, \mu_+ > 0$, whereas $\gamma < 0$ for negative index materials.

The total electromagnetic fields $u_\pm$ are given by

$$\begin{aligned} u_+ &= u^i + (\mathbf{E}_+, \mathbf{H}_+), \quad \text{in } G_+, \\ u_- &= (\mathbf{E}_-, \mathbf{H}_-), \quad \text{in } G_-, \end{aligned} \tag{2}$$

and satisfy: quasiperiodicity by a multiplication operator $F_{\alpha,\beta}$ acting on (α, β)-quasiperiodic function $u:\mathbf{R}^3 \to C$ such that

$$F_{\alpha,\beta}\, u(\mathbf{r}) := \exp[i(\alpha x + \beta y)]\, u(\mathbf{r}); \tag{3}$$

the outgoing wave conditions in the sense of Rayleigh series with coefficients $c^{\pm}_{n,m}$,

$$\begin{aligned} u_+ - u^i &= \sum_{n,m=-\infty}^{\infty} c^{+}_{n,m} \exp\bigl[i(\alpha_n x + \beta_m y + \gamma^{+}_{n,m} z)\bigr], \quad z \geq 0, \\ u_- &= \sum_{n,m=-\infty}^{\infty} c^{-}_{n,m} \exp\bigl[i(\alpha_n x + \beta_m y - \gamma^{-}_{n,m} z)\bigr], \quad z \leq -h, \end{aligned} \tag{4}$$

where $\alpha_n = \alpha + 2\pi n/d_x$, $\beta_m = \beta + 2\pi m/d_y$ and $\gamma^{\pm 2}_{n,m} = k^2_{\pm} - \alpha^2_n - \beta^2_m$ with $\gamma^{\pm}_{n,m} > 0$ or $-i\gamma^{\pm}_{n,m} > 0$; and also boundary conditions for the tangential components of $\mathbf{E}$, $\mathbf{H}$, curl $\mathbf{E}$ and curl $\mathbf{H}$,

$$\begin{aligned} [\mathbf{n} \times u]_{\partial\Omega_{\pm}} &= 0, && \text{for } \mathbf{E} \text{ and } \mathbf{H}, \\ [\mathbf{n} \times \hat{\mu}^{-1}(\nabla \times \mathbf{E})]_{\partial\Omega_{\pm}} &= 0, && \text{for } \nabla \times \mathbf{E}, \\ [\mathbf{n} \times \hat{\epsilon}^{-1}(\nabla \times \mathbf{H})]_{\partial\Omega_{\pm}} &= 0, && \text{for } \nabla \times \mathbf{H}. \end{aligned} \tag{5}$$

The square brackets in (5) denote the jump of functions across $\Gamma_{\pm}$.

Using (4) for the field and its normal derivative representations on $\Gamma_{\pm}$, equation (5) can be transformed to the form of nonlocal transmission conditions (see, for example, Dobson, 1994), which satisfy

$$\begin{aligned} \partial_z u(x, y, 0) &= -T^{+}_{\alpha,\beta}\, u(x, y, 0) - 2\mathrm{i}\beta p, \\ \partial_z u(x, y, -h) &= T^{-}_{\alpha,\beta}\, u(x, y, -h), \end{aligned} \tag{6}$$

where

$$T^{\pm}_{\alpha,\beta}\, u(x, y) = \sum_{n,m=-\infty}^{\infty} -i\gamma^{\pm}_{n,m}\, c^{\pm}_{n,m} \exp\bigl[i(\alpha_n x + \beta_m y)\bigr], \tag{7}$$

with the Fourier coefficients

$$c^{\pm}_{n,m} = \frac{1}{d_x d_y} \int_{\Gamma} u(x, y) \exp\bigl[-i(\alpha_n x + \beta_m y)\bigr]\, \mathrm{d}x\, \mathrm{d}y.$$

The pseudodifferential operators $T^{\pm}_{\alpha,\beta}$ acting on doubly periodic vector functions on $\mathbf{R}^2$ specify the Dirichlet-to-Neumann map. The operators $T^{\pm}_{\alpha,\beta}$ map the Sobolev space $H^s_p(\Gamma)$ of doubly periodic functions defined on Γ boundedly into $H^{s-1}_p(\Gamma)$, $s \in \mathbf{R}$. The equality in (7) is valid in the sense of distributions. The space $H^s_p(\Gamma)$ denotes the closure of smooth doubly periodic functions on $\mathbf{R}^2$ with respect to the norm,

$$\left(|c_{0,0}|^2 + \sum_{n,m=-\infty\setminus\{0,0\}}^{\infty} |(n, m)|^{2s} |\, c_{n,m}|^2 \right).$$

Note that $H^s_p(G)$ denotes the restriction to G of all doubly periodic functions in $H^s_{\mathrm{loc}}(\mathbf{R}^3)$, and for $u \in H^1_p(G)$ the boundary values $u|_{\Gamma_{\pm}} \in H^{1/2}_p(\Gamma_{\pm})^3$.

In the following we need vector fields $\mathbf{E}_{\pm}, \mathbf{H}_{\pm}$ of locally finite energy

$$\mathbf{E}_{\pm}, \mathbf{H}_{\pm}, \nabla \times \mathbf{E}_{\pm}, \nabla \times \mathbf{H}_{\pm} \in \mathbf{L}^2_{\mathrm{loc}}(G)^3$$

that is enough to satisfy Meixner's edge condition (Li, 2014) and two couples of time-harmonic Maxwell equations without exterior current [it is also valid for metamaterials; see, for example, Popov (2014, ch. 12) and Bugert & Schmidt (2015)],

$$\nabla \times \mathbf{E} = i\omega \mathbf{B}, \qquad \nabla \times \mathbf{H} = -i\omega\, \mathbf{D}, \tag{8}$$

$$\mathbf{D} = \epsilon_{\mathrm{v}} \hat{\epsilon}\, \mathbf{E}, \qquad \mathbf{B} = \mu_{\mathrm{v}} \hat{\mu}\, \mathbf{H}, \tag{9}$$

where ϵ_{v} and μ_{v} are vacuum constants. Thus, equations introduced in (8) and (9) together with (1)–(7) give us the full problem statement.

3. Power balance, absorption and scattering intensity formulae

3.1. Power balance

The efficiency of a diffracted or transmitted propagating mode (order) represents the proportion of power radiated in each order. Defining the power for time-harmonic electromagnetic incident fields as the flux density of the Poynting vector modulus $|\mathbf{S}^i| = \mathrm{Re}\,(\mathbf{E}^i \times \overline{\mathbf{H}^i})/2$ ($\overline{C}$ means here the complex conjugate of C) through a normalized rectangle parallel to the (x, y)-plane (Fig. 2), the ratio of the power of reflected or transmitted propagating orders and of the incident wave gives the sum of diffraction efficiencies of reflected orders R or transmitted orders T. Diffraction efficiencies for the reflected and transmitted orders of any grating can easily be found from the corresponding Rayleigh coefficients or boundary values (Popov, 2014). If a general multilayer grating (Fig. 1) has the perfectly conducting substrate, *i.e.* $\nu_N = (0, \infty)$, where ν_N is a refractive index in the substrate and there is not any power absorption in the grating layers, $\mathrm{Im}\,\hat{\nu}_j = 0$, where $\hat{\nu}_j$ are refractive index matrices, $j = 1, \ldots, N-1$; then energy conservation under unitary normalization for the incident wave is expressed by the standard energy criterion $R = 1$. If the grating is lossless, $\mathrm{Im}\,\hat{\nu}_j = 0$, $j = 0, \ldots, N$, then power conservation is expressed by a similar energy balance criterion $R + T = 1$. In most publications devoted to the theory of diffraction gratings (*e.g.* Popov, 2014), one verifies power conservation by calculating the real part of a surface integral over the lossless grating region for the normal component of Poynting's vector $\mathbf{S} = \mathbf{E} \times \overline{\mathbf{H}}/2$,

$$R + T - 1 = \mathrm{Re} \oint \mathbf{S}\mathbf{n}\, \mathrm{d}s = 0. \tag{10}$$

If $\mathrm{Im}\,\hat{\nu}_j > 0$ for some $j = 1, \ldots, N$, then there is some energy absorption in the grating layers or/and in the substrate. Thus, the above-mentioned principle of power conservation, that the sum of efficiencies of all reflected and transmitted orders should be equal to the power of the incident wave, does not hold. In a general case,

$$A + R + T = 1, \tag{11}$$

where A is called the absorption coefficient or simply the absorption in the given diffraction problem. In the lossy case,

an independently calculated quantity A is required to verify (11). In particular, the values of the field on Γ_+ and Γ_- can give valuable information on the absorbing power. To find such a quantity a valid approach should be used because some arbitrariness exists in the definition of **S** as well in the calculation of the surface integral in (10) (Born & Wolf, 2002). Besides, knowledge of a directly calculated value of the absorption for a grating is a useful and self-consistent tool for single-computation testing the correctness and reliability of developed computer codes. In many difficult cases convergence of A has to be compared with convergence of indirect absorption calculus,

$$A_i = 1 - R - T, \tag{12}$$

that can be derived also from measurements of R and T. Due to numerical differences in the concrete rigorous method to compute near- and far-zone fields, the differences between direct and indirect absorbtion calculations sometimes can be big enough (Popov, 2014; Goray *et al.*, 2006*a*,*b*).

3.2. Bi-periodic diffraction grating

The present formulation for the power balance and absorption coefficient of anisotropic inhomogeneous bi-gratings follows the classical line on the variational and integral-equation approaches applying to the diffraction problem formulation. Suppose from the literature (*i.e.* Dobson & Friedman, 1992; Dobson, 1994; Bao *et al.*, 1995; Bao, 1997; Bao & Dobson, 2000; Schmidt, 2003; Bugert & Schmidt, 2015) that **E**, **H** are a solution of the partial differential formulation of the diffraction problem (1)–(9), the expression for the power balance and absorption can be derived from Maxwell's equations for curl **E** and curl **H** in a periodic cell G, which has in the x-direction the width d_x, in the y-direction the width d_y and is bounded by planes $z = 0$, $z = -h$ and contains Γ. A simple derivation of the expression for direct absorption calculus in quadratures is demonstrated by Goray (2015). The absorption integral generalized by Goray (2015) for a lossy bi-periodic grating is expressed using conductivity tensors and the fields on the surface restricting a grating domain between uniform medias as

$$A_2 = \frac{\left(\mu_+/\epsilon_+\right)^{1/2}}{2d_x d_y \cos\theta}\ \mathrm{Im} \int\limits_{\Omega} \overline{\mathbf{E}}\,\hat{\sigma}_\mathrm{e}\,\mathbf{E} + Z_\mathrm{v}^2\,\overline{\mathbf{H}}\,\hat{\sigma}_\mathrm{m}\,\mathbf{H}\ \mathrm{d}v. \tag{13}$$

where Z_v is the vacuum impedance (Born & Wolf, 2002), $\hat{\sigma}_\mathrm{e} = \omega\epsilon_\mathrm{v}(\tilde{\epsilon} - \hat{\epsilon})/2$, $\hat{\sigma}_\mathrm{m} = \mu_\mathrm{v}\omega(\tilde{\mu} - \hat{\mu})/2$ are electric and magnetic, respectively, conductivity tensors and $\tilde{\epsilon}$ and $\tilde{\mu}$ are hermitian conjugates to tensors $\hat{\epsilon}$ and $\hat{\mu}$ (*e.g.* obtained by a matrix transposition and complex conjugations of matrix elements), respectively. Formula (13) describes the Joule effect losses density in the absorbing bi-periodic grating and the normalization coefficient includes the diffraction problem parameters.

Equation (13) represents the main result for the absorption of any bi-grating described above and is used in the normalized energy balance of equation (11) to test numerical codes. It is valid for any rigorous electromagnetic method which can derive local values of **E** and **H** in the volume of one grating period. Such a directly calculated absorption can be (and should be) compared with the indirect value of A_i to check the accuracy of results. However, for some rigorous approaches such as boundary integral equation methods, boundary element methods and methods of fictitious sources, surface integrals are much more preferable to calculate. For such numerical methods, direct calculus of A using a surface (or contour, for one-gratings) integral for the Pointing vector component over the closed grating region can be used. It reads by (13) as

$$A_2 = \frac{Z_\mathrm{v}\left(\mu_+/\epsilon_+\right)^{1/2}}{2d_x d_y \cos\theta}\ \mathrm{Re} \int\limits_{\partial\Omega} \mathbf{E} \times \overline{\mathbf{H}}\,\mathbf{n}\ \mathrm{d}s. \tag{14}$$

The general existence and uniqueness of a solution for A formally results immediately from the strong ellipticity concept via the variational and integral-equation formulations for **E** and **H** derived from the above-mentioned rigorous mathematical studies. If the structure contains absorbing materials and the permittivity tensors are piecewise analytic, as it is in all the practical cases considered in this paper, then the diffraction problem is uniquely solvable for all frequencies (Schmidt, 2003).

3.3. One-periodic diffraction grating

For one-periodic gratings very similar results for the absorption A_1 can be obtained on the basis of the respective integral-equation and/or weak formulation proofs (Popov, 2014, chs. 5, 12; Bao *et al.*, 1995) and taking into account that the field does not vary in one coordinate. The volume integral should be exchanged with the surface one for a rectangle surface Γ' of area $d_x h$ and with the new normalization for the incident power,

$$A_1 = \frac{\left(\mu_+/\epsilon_+\right)^{1/2}}{2d_x \cos\theta}\ \mathrm{Im} \int\limits_{\Gamma'} \overline{\mathbf{E}}\,\hat{\sigma}_e\,\mathbf{E} + Z_\mathrm{v}^2\,\overline{\mathbf{H}}\,\hat{\sigma}_\mathrm{m}\,\mathbf{H}\ \mathrm{d}s. \tag{15}$$

Popov 's derivation (Popov, 2014, ch. 12) of the energy balance and A_1 for isotropic one-periodic gratings working in classical or conical (azimuthal angle $\phi \neq 0$) diffraction (Fig. 1) is based on computations of the respective contour integrals by values of the fields $E(x, y, z) = E(x, y)\exp(i\gamma z)$ and $U(x, y, z) = Z_\mathrm{v}H(x, y)\exp(i\gamma z)$, $\gamma = \omega(\epsilon_+\mu_+)^{1/2}\sin\phi$ and their normal (∂_n) and tangential (∂_t) derivatives on a grating boundary Γ,

$$A_1 = \frac{1}{\beta}\,\mathrm{Im}\left[\frac{\kappa_+^2}{\kappa_-^2}\left(\frac{\varepsilon_-}{\varepsilon_\mathrm{v}}\int\limits_{\Gamma'} \partial_n^- E_z \overline{E}_z + \frac{\mu_-}{\mu_\mathrm{v}}\int\limits_{\Gamma'} \partial_n^- U_z\,\overline{U}_z\right.\right.$$
$$\left.\left. + \left(\frac{\epsilon_+\mu_+}{\epsilon_\mathrm{v}\mu_\mathrm{v}}\right)^{1/2} 2\sin\phi\ \ \mathrm{Re}\int\limits_{\Gamma'} E_z\,\partial_t^-\,\overline{U}_z\right)\right], \tag{16}$$

where $\kappa_\pm = \epsilon_\pm\mu_\pm - \epsilon_+\mu_+\sin\phi$ in the upper (+) and lower (−) mediums, $\epsilon_\pm$ and $\mu_\pm$ are electric permittivities and magnetic permeabilities, respectively, β is the wavevector y-component, **n** is the outward unit vector of the normal, and arc length

integration is performed assuming $d = 1$ along one period Γ of the cut of the boundary by the $z = 0$ plane.

For multilayer gratings, A_1 is similarly calculated as the difference between energy flux densities, which cross the upper, Γ_0, and the lower, Γ_{N-1}, boundaries of the multilayer structure through cells $G_{\pm H}$ bounded by planes $x = 0$, $x = d$, $z = 0$, $z = 1$, $y = \pm H$ and contained Γ_0 or Γ_{N-1},

$$A_1 = \frac{1}{\beta}\,\mathrm{Im}\left[\int\limits_{\Gamma_0}\left(\frac{\epsilon_+}{\epsilon_\mathrm{v}}\,\partial_n^+ E_z\,\overline{E}_z + \frac{\mu_+}{\mu_\mathrm{v}},\partial_n^+ U_z\,\overline{U}_z\right) - \frac{\kappa_+^2}{\kappa_-^2}\int\limits_{\Gamma_{N-1}}\left(\frac{\varepsilon_-}{\varepsilon_v}\,\partial_n^- E_z\,\overline{E}_z + \frac{\mu_-}{\mu_\mathrm{v}}\,\partial_n^- U_z\,\overline{U}_z\right)\right], \quad (17)$$

where $\mathbf{n}_0$ and $\mathbf{n}_{N-1}$ are unit vectors of the normal, which are interior to the regions under study.

From the detailed mathematical analysis of the conical diffraction solution using boundary integral equations, the Fredholmness of operators V^+ and V^-, *i.e.* which are bounded linear operators between two Banach spaces, has been established with the basic properties (Popov, 2014, ch. 12).

3.4. Random 2D surface

Here we use the model in which an uneven surface is represented by a bi-grating with large periods of d_x, d_y in perpendicular planes, which include appropriate numbers of random asperities with correlation lengths of ξ_x and ξ_y, respectively. We analyze a complex structure which, while being the multilayer bi-grating from a mathematical viewpoint, is actually the rough surface for $d_x, d_y \gg \xi_x, \xi_y$. If $\xi_x, \xi_y \simeq \lambda$ and the number of modes (orders) is large, the continuous angular distribution of the power reflected or transmitted from random boundaries can be described by a discrete efficiency distribution $\eta_{n,m}$ in orders $(n, m) \in \mathbf{Z^2}$ of a bi-grating, similar to that reported by Goray (2010*b*) to present random 1D surfaces using classical gratings. As the ensemble size increases, the results converge to the statistical moment using $\sim 10\xi_{x,y}$ or more per $d_{x,y}$ that depends on statistical properties of rough surfaces (Warnick & Chew, 2001; Saillard & Sentenac, 2001). In this section the author describes an approach applicable for general 2D surfaces that generalizes the methods (Popov, 2014, ch. 12; Goray, 2010*b*) developed to study the scattering intensity (diffraction efficiency), absorption and power balance of general 1D surfaces and randomly rough one-periodic gratings.

Let $\mathbf{E}$ and $\mathbf{H}$ be a solution of the partial differential formulation of the deterministic diffraction problem stated above. The expression for the energy balance for random 2D surfaces was derived (Goray, 2016) using statistical averaging. By the definition of the bistatic scattering coefficients (BSCs) $\zeta^\pm$ for the reflected (+) and transmitted (−) powers (Tsang *et al.*, 2001) and using the definition for the normalized incident power (Schmidt, 2003) one can formulate the energy conservation law for random 2D surfaces,

$$1 - \left\langle \sum_{\gamma_{n,m}^+ > 0} \eta_{n,m}^+ \right\rangle - \left\langle \sum_{\gamma_{n,m}^- > 0} \eta_{n,m}^- \right\rangle - A = 0, \quad (18)$$

where A is a mean absorption value averaged out over all statistical realizations,

$$A = \frac{\left(\mu_+/\epsilon_+\right)^{1/2}}{2d_x d_y \cos\theta}\left\langle \mathrm{Im}\int\limits_G \overline{\mathbf{E}}\,\bar{\sigma}_\mathrm{e}\,\mathbf{E} + Z_\mathrm{v}^2\,\overline{\mathbf{H}}\,\bar{\sigma}_\mathrm{m}\,\mathbf{H}\,\mathrm{d}v\right\rangle. \quad (19)$$

Formula (19) can be expressed using a surface integral for the Poynting vector component over the closed grating region Γ, similarly to (14),

$$A_2 = \frac{Z_\mathrm{v}\left(\mu_+/\epsilon_+\right)^{1/2}}{2d_x d_y \cos\theta}\left\langle \mathrm{Re}\int\limits_\Gamma \mathbf{E}\times\overline{\mathbf{H}}\,\mathbf{n}\,\mathrm{d}s\right\rangle. \quad (20)$$

A study of the scattering intensity by the Monte Carlo method starts with obtaining statistical realizations of profile boundaries of the structure to be analyzed, after which one calculates $\zeta^\pm$ for random realizations. For $\lambda/d_{x,y} \ll 1$ the discrete order efficiencies $\eta_{n,m}^\pm$ are approximations of BSCs for a continuum of scattered angles $\theta_{n,m}^\pm$, $\phi_{n,m}^\pm$ in G_+ and G_- (if exist) mediums. Then, efficiencies are averaged out over all realizations to obtain a mean BSC $\tilde{\zeta}$ measured in real experiments,

$$\left\langle \sum_{\gamma_{n,m}^\pm > 0} \eta_{n,m}^\pm \right\rangle = \int\limits_{-\pi/2}^{\pi/2}\int \tilde{\zeta}\left(\theta_{n,m}^\pm, \phi_{n,m}^\pm\right)\mathrm{d}\theta_{n,m}^\pm\,\mathrm{d}\phi_{n,m}^\pm. \quad (21)$$

Finally, using (21) and (18) the generalization of the normalized power balance for random lossy 2D surfaces can be represented as

$$\int\limits_{-\pi/2}^{\pi/2}\int \tilde{\zeta}\left(\theta_{n,m}^\pm, \phi_{n,m}^\pm\right)\mathrm{d}\theta_{n,m}^\pm\,\mathrm{d}\phi_{n,m}^\pm + A = 1, \quad (22)$$

where the direct expression for one realization of ζ is given by Goray (2016) and A is calculated in quadratures as (19) or (20). By selecting large enough samples and numbers of sampling points, one comes eventually to properly averaged properties of the rough surface. There are not any approximations in such an approach, except restrictions of the numerical realization. The similar expression of $\zeta^\pm$ for 1D random surfaces is presented by Popov (2014, ch. 12).

4. Examples of X-ray absorption and scattering intensity calculus

The numerical implementation approach expedient for the calculation of near-fields, far-fields and polarization features of classical or conical diffraction by one-periodic gratings and general diffraction by bi-periodic gratings working in the entire optical wavelength range was described in the earlier publications (Goray & Schmidt, 2010, 2012; Goray & Egorov, 2016; Popov, 2014; Bugert & Schmidt, 2015). Here the author presents several numerical experiments taken from important applications of gratings and rough surfaces working in X-ray–EUV ranges. Using the above-described methods, the present

results demonstrate the impact of the rigorous approach on: (1) the absorption in the multilayer W/B_4C blaze grating working in classical and conical soft-X-ray mounts; (2) the scattering by the flight rough multilayer Mo/Si trapezoid grating working in the EUV range; (3) the absorption in 1D rough GaAs substrates illuminated by hard X-rays; (4) the scattering by the rough 2D Au surfaces working in the soft X-ray range. Examples of the found absorption and scattering coefficients for gratings and mirrors working in X-rays are compared with those derived using the usual indirect approach and well known approximations. The refractive indices of the materials were taken from the CXRO website (CXRO, 2020).

4.1. Absorption of a multilayer blaze grating working in classical and conical mounts

Multilayer-coated blazed gratings with high groove densities are the best candidates for use in high-resolution X-ray and EUV spectroscopy including RIXS (Voronov *et al.*, 2015). Theoretical and experimental analysis show that such a grating can be potentially optimized for high dispersion and spectral resolution in a desired high diffraction order without significant loss of diffraction efficiency. In order to realize this potential, the grating should have a near-perfect triangular groove profile and its absorption should be minimized. The grazing-incidence conical-diffraction mounting in which the direction of incident light is confined to a plane parallel to the direction of the grooves has the unique property of maintaining high and sustained diffraction efficiency due to an additional angular parameter (Goray & Egorov, 2016). In this section, we analyze the optical absorption of a blazed multilayer grating working in the equivalent grazing classical and conical diffraction mounts in the soft X-ray range.

In Fig. 3 the absorption of the 114.3 nm-period blazed Si grating coated with 50 bi-layers of W/B_4C working in classical ('classic') and conical ('conic') mounts was calculated for the TE and TM polarized incidence radiation as a function of λ. For the classical mount, $\theta = 83.25^\circ$ and the azimuthal angle $\phi = 0$. For the conical mount, $\theta = 6^\circ$ and the azimuthal angle $\phi = 77.24$. The grating has a triangular groove profile with a blaze angle of 6° (-4th blazed order) and antiblaze angle of 64.53° and a conformal multilayer coating with the same thickness of 1.5 nm of W and B_4C layers. For gratings in the grazing-incidence off-plane mount, we refer to linearly polarized incident light whose electric field vector lies in the plane of incidence as the TE polarization (p), and define the TM polarization (s) as when the electric field vector lies almost parallel to the plane of the grating (Marlowe *et al.*, 2016). Fig. 3 displays for comparison theoretical absorption spectra of a Si mirror coated with the same multilayer and working at the optimal grazing incidence.

As one can see in Fig. 3, for the defined polar and azimuthal angles the conical grating and mirror absorption spectra are close in the wavelength range investigated. The grating absorption minima ~73% can be obtained for the optimal wavelength of ~1.288 nm (s polarization). Thus, almost all the

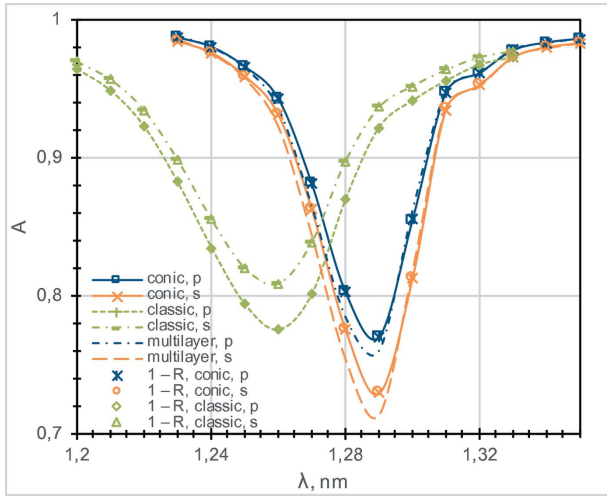

Figure 3
Absorption of the W/B_4C multilayer blazed diffraction grating working in conical ('conic') or classical ('classic') mount calculated for the TE ('p') and TM ('s') polarized incident radiation versus wavelength. '$1 - R$' are non-direct absorption calculations.

reflected energy in this mount can be directed into the principal diffraction order without additional losses for the grating absorption. In contrast, the best in-plane value of A calculated at $\lambda \simeq 1.26$ nm is ~7% higher. The absorption spectral dependence calculated using the indirect method exhibits a minor difference, less than 1%, in the vicinity and around the absorption minima. That is, mostly, due to inaccurate calculus of higher-order efficiencies in the indirect approach.

Only $\mathcal{N} = 400$ were used to compute this grating example which allocates ~60 MB of RAM. The relative error calculated from the energy balance using (11) is $\sim 10^{-3}$. The average time taken up by one point on a portable workstation MSI WT73VR 7RM with an Intel® Xenon® E3-1505M V6 and 3–4 GHz processor and 64 GB of RAM is ~2 min when operating on Windows® 10 Pro.

4.2. Scattering intensity of a flight Mo/Si multilayer rough trapezium grating in the EUV

Examples of the Mo/Si lamellar-type grating efficiency and scattering light intensity computations were carried out for the Extreme-Ultraviolet Imaging Spectrometer (EIS) on the Hinode (former Solar-B) mission (Hinode, 2020), the first implementation of a multilayer grating on a satellite instrument. For today, the mission duration elapsed is about 14 years instead of the initially planned three-year mission. Here we present the efficiency (of orders) and scattered light intensity (between orders) calculus of the flight FL1 4200 grooves mm^{-1} multilayer-coated grating operating at $\theta = 6.5^\circ$ of the in-plane configuration for a wavelength of 19.25 nm in the working wavelength region 17–23 nm (Fig. 4). The efficiency was directly calculated by boundary-integral-equation software (PCGrate®-SX v. 6.6; IIG, 2020) using data of AFM measurements and accounting for the random roughness. The results of computations agree well with synchrotron

efficiency measurements (Popov, 2014, ch. 12). The calculated scattering light intensity between the orders is about 1000 times lower than the −1 order minimal efficiency that is in a quantitative agreement with the measured level.

The depth of all the boundary profiles of the multilayer grating was ∼6.0 nm, with side slopes of 35° and equal top and groove widths, as derived from the AFM and efficiency measurements. Because polarization effects are small near normal incidence, the efficiencies are presented for the case of TM-polarized radiation. To determine the absolute values of the scattering intensity, a model of the two-period randomized-trapezium grating describing the realistic boundary shape and roughness was applied. For a rigorous accounting of the random roughness impact on the efficiency, a model with 41 randomly rough borders of the period of ∼476.19 nm having 400 random sampling points on two trapezoidal grooves with the same Gaussian surface roughness height statistics and the Gaussian autocorrelation function was applied. The rough boundary parameters are as follows: the Si–Mo interface r.m.s. roughness $\sigma_{\mathrm{Si–Mo}} = 0.2$ nm and the Mo–Si r.m.s. roughness $\sigma_{\mathrm{Mo–Si}} = 0.85$ nm. The lateral correlation length $\xi = 5$ nm was chosen from the detailed microscopic analysis and the growth model of typical Mo/Si layers obtained by using magnetron sputtering (Goray & Lubov, 2013). An assumption about the absence of a vertical correlation between the border random roughness components was applied in this model. Seven sets of 41 rough border profiles were generated to compute the exact efficiency and scattering light intensity of the FL1 multilayer grating. The Si protective capping layer of 2 nm was modeled by using 1.5 nm-thick amorphous SiO_2 on 1.5 nm Si in order to account for the oxidation of the Si capping layer. The FL1 multilayer parameters extracted from the mirror investigation are as follows: 20 Mo/Si layer pairs with the bilayer period $D = 10.3$ nm, Mo thickness to D ratio $\Gamma = 0.37$.

A medium rate of convergence of the light intensity results was observed for a wavelength of 19.25 nm and the above computation model. About 100 random sets of 41 rough border profiles and the medium number of discretization points (800–1200) are enough to compute exact values of scattering light intensities between orders. The difference between efficiencies obtained using medium ($N = 1000$) and high ($N = 1200$) accuracy is about 10^{-5} for almost all diffraction orders. The scattered light intensities were calculated with different numbers of statistical boundary sets (35, 70, 98, 105) and $N = 1000$ for all diffraction (scattering) angles. The differences between scattering light intensities obtained with 98 and 105 statistical boundary sets are about 10^{-6}. For the final scattering intensity modeling, $N = 1000$ and 105 random boundary sets were chosen. The error derived from the energy balance was about 10^{-5} for all computation points and random sets. The time taken up by one rigorous computation (one random set) for $N = 1000$ on the aforementioned workstation and operating system is ∼12 min.

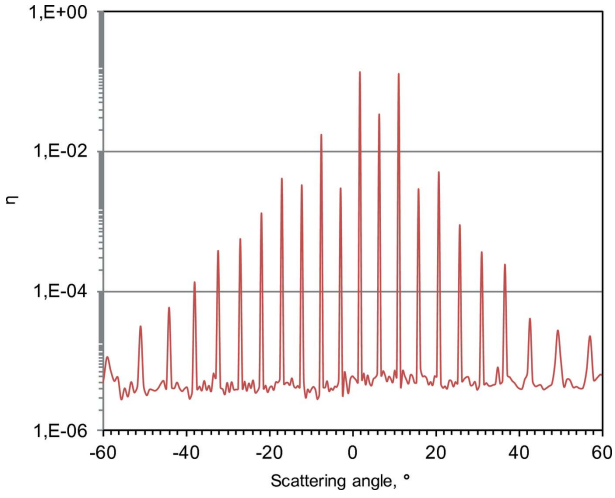

Figure 4
Scattering intensity of the Mo/Si multilayer-coated randomly rough lamellar grating in the EUV versus scattering angle.

4.3. Absorption in rough GaAs substrates

Rigorous computations of the absorption in rough GaAs substrates were performed using the method of deep X-ray reflectometry (DXRR) (Goray *et al.*, 2019, 2020). That new approach in the short-wave scatterometry (Goray, 2009) is based on the rigorous theory of diffraction of electromagnetic radiation, *i.e.* the boundary integral equation method using the method of Monte Carlo, or microscopic images, or growth model data of realistic surfaces to take into account boundary irregularities (Goray & Lubov, 2013, 2015; Goray *et al.*, 2009, 2010). It can describe different situations from total external reflection to full absorption of short-wave radiation; in addition to specular reflectances, it enables accurate determination of the intensity of scattered light and absorption. For example, the big differences, in orders of magnitude, between the rigorous approach and the Debye–Waller (DW) and Nevot–Croce (NC) approximations were firstly demonstrated in specular reflectances of Au mirrors with different roughness parameters at wavelengths where grazing incidences occur at close to or larger than the critical angles (Goray, 2010*b*).

It is known that the second-order distorted-wave Born approximation (DWBA) and the height perturbation theory may be used accounting for any correlation length and more general rough statistics (Goray *et al.*, 2020). However, all approximations have strong restrictions, mainly in the allowed maximal values of σ (Ogilvy, 1987; Stearns, 1992; de Boer, 1996; Kozhevnikov & Pyatakhin, 1998). In particular, for specular reflection the DWBA model is generally valid for very small values of σ and ξ when the Gaussian-like correlation function is used: $\sigma \ll \lambda/(2\pi \sin\theta)$ and $\xi \ll \lambda/(2\pi \sin^2\theta)$. The case of diffuse scattering is even more complex and the result depends also significantly on real rough statistics (Saillard *et al.*, 1986).

To investigate examples of GaAs surfaces we used the interface roughness with the Gaussian height statistics and the Gaussian autocorrelation function. Different values of σ were applied to generate boundary samples: 0.35 nm, 0.7 nm and 1.5 nm. Various correlation lengths evaluated had values close

to those given by either the DW model ($\xi = \infty$) or the NC model [or more general Sinha's approximation (Sinha *et al.* (1988)] ($\xi = 0$), or more realistic models ($\xi = 0.15$, 1.5, 15 μm) in the entire grazing-incidence angle range. The calculated TE absorption (TM absorption data are close in magnitude) of GaAs surfaces versus grazing angle of incidence for different values of σ and ξ is shown in Fig. 5. We discuss here only the behavior of exact and approximate values of the absorption when the grazing-incidence angle is close to the critical angle. For $\xi = 0.15$ μm, the absorption calculated for the rigorous and NC model differ only by a few percent near and below the critical angle, and by several percent in the range slightly higher than the critical angle. For $\xi = 1.5$ μm, the difference is several percent in the low absorption range, and approximately a few tens of percent in the high absorption range. For $\xi = 15$ μm, the difference is about a few tens of percent in the low absorption range, and approximately several tens of percent or a few times in the high absorption range; similar differences can be observed for $\xi = 15$ μm and the DW model. For $\sigma = 0.7$ nm, the NC model absorption (not shown) is close (with the maximal difference of several percent) to the absorption of the perfect surface, and also to the rigorous model absorption with the highest value of $\xi = 15$ μm. For $\sigma = 0.35$ nm, all the models are very close (with the maximal difference of only a few percent) in the working incidence angle range. Thus, the exact results for small values of σ and ξ are close to the NC model near and slightly below the critical angle, in accordance with de Boer (1996). For higher than ~0.35 nm values of σ, big differences between the rigorous model and any widely used approximations may result in a non-correct estimation of the absorption. For higher grazing-incidence angles the absorption is higher, the reflectance is lower and the difference between the rigorous and asymptotic models may increase many times (Goray, 2010*b*; Goray *et al.*, 2020).

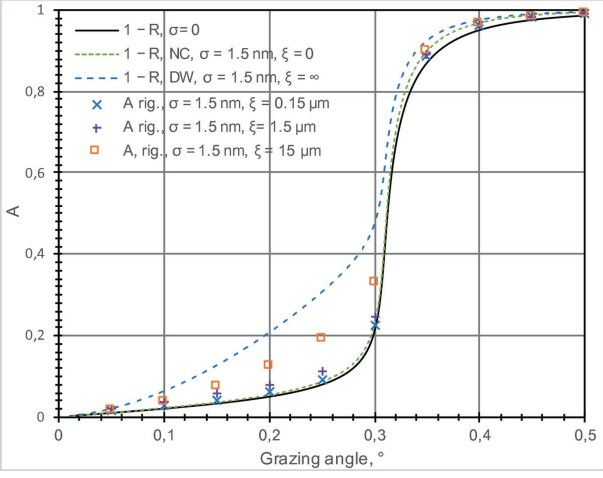

Figure 5
Absorption of GaAs versus grazing-incidence angle. Absorption calculated by approximations (NC or DW curves) and rigorously (symbols) with 99 statistical surface realizations for $\lambda = 0.1541$ nm and different r.m.s. roughness σ and correlation length ξ. '$1 - R$' are non-direct absorption calculations using approximations.

The results presented in Fig. 5 exhibit moderate convergence and high accuracy required for simulating absorption of GaAs random surfaces. In PCGrate, we used 1000–1200 discretization points per boundary, 99–195 random surface sets, and the scattering matrix approach (IIG, 2020). An error of about 10^{-6} was estimated from the energy balance. The difference between absorptions obtained using 99 and 195 random surface sets is approximately 0.1%. The difference between absorptions obtained using 49 and 195 random surface sets is approximately (or less than) 10%. The average time taken by each discretization point (99 random sets) on the mentioned portable workstation is approximately four hours when operating on Windows® 10 Pro using eightfold parallelization.

4.4. Scattering intensity of Au 2D rough surfaces with different correlation functions

Here we study the influence of 2D surface topology of a continuum Au film on short-wave scattering intensity, *i.e.* the bistatic scattering coefficient (Tsang *et al.*, 2001). With this last example, η of mirrors with different types of rough statistics working at a wavelength of 1.54 nm are calculated using the equivalence formulae for orthogonal planes (Goray, 2013). Two types of Au mirrors have the same models of roughness in different directions [(yOz) and (xOy) planes], which are approaching closely the typical realistic conditions: (1) having a Gaussian height distribution with $\sigma_{x,z}$ and a Gaussian autocorrelation function $C_{x,z} = \sigma_{x,z} \exp[(x, z)^2/\xi_{x,z}^2]$; (2) having the same Gaussian height distribution and an exponential autocorrelation function $C_{x,z} = \sigma_{x,z} \exp[(x, z)/\xi_{x,z}]$ with $\sigma_x = \sigma_z = \sigma$ and $\xi_x = \xi_z = \xi$. Statistical surface realizations with $\sigma = 1$ nm, $\xi = 15$ nm and the different correlation functions were generated using the spectral method (Tsang *et al.*, 2001).

In Fig. 6, η(TE) (the vector of the electric field is perpendicular to the incident plane) of Au mirrors is plotted versus reflection grating order number (angle of scattering) in perpendicular planes for the incident angle of $\theta = 87°$ which is beyond the critical angle at a wavelength $\lambda = 1.54$ nm. Note that the TM values of η, as well as the respective Fresnel coefficients, are very close to the TE values for both types of statistics. As follows from a comparison of the curves shown in Fig. 6, $\eta_{0,n}$ corresponding to the (yOz) plane is much higher, beyond the specular reflection, than $\eta_{m,0}$, which are related to the (xOy) (incident) plane. Moreover, $\eta_{0,n}$ are, roughly, symmetric functions with respect to specular peaks, while $\eta_{m,0}$ depend on negative order numbers only due to the grazing-incidence geometry. The diffuse reflection coefficients of the model with the exponential autocorrelation function mostly exceed the corresponding coefficients of the model with the Gaussian autocorrelation function in the (yOz) plane. In the (xOy) plane, $\eta_{m,0}$ for the Gaussian autocorrelation function has a smooth incline, without significant fluctuations, opposite to the exponential autocorrelation function. Such behaviors are due to the higher noisiness of boundaries with the exponential autocorrelation function. Thus, the observed discrepancies between the angle dependences of scattering

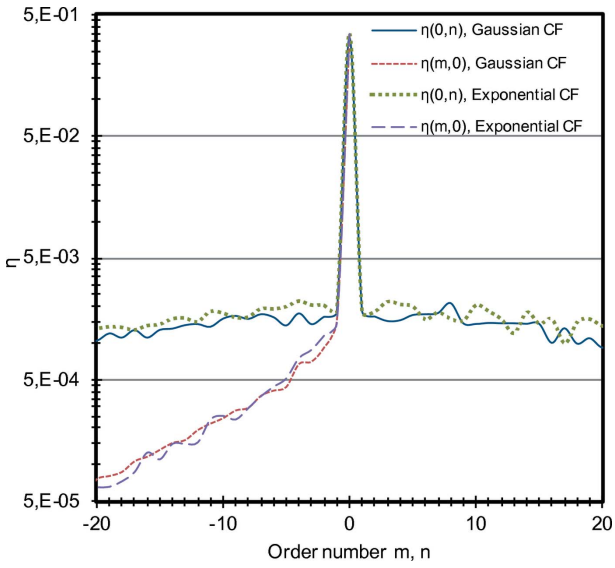

Figure 6
Scattering intensity of an Au mirror having Gaussian roughness with σ = 1 nm, ξ = 15 nm and indicated correlation function (CF) for radiation incident at $\lambda = 1.54$ nm and $\theta = 87°$ versus diffraction order number m or n.

intensities of mirrors with similar surface topologies indicate that, in practice, critical samples must be calculated with the help of an accurate roughness model.

To obtain the required ensemble averaging and calculation accuracy for rough surfaces, 100–200 statistical sets have to be used with 1000 node points within a 1 μm interval $d_x = d_z = d$ on each. To take into account the fine structure of the rough surface and low convergence of the results obtained, we chose the number of discretization points N = 2000 and ∼200 statistical sets in the PCGrate®-SX v.6.7 code. An error of about 10^{-5} was estimated from the energy balance. The average time taken by one calculation (198 random sets) on the mentioned portable workstation is ∼13 h using eightfold parallelization.

5. Summary and conclusions

The generalized power balance for structured interfaces allows direct calculus of light absorption and scattering using expressions derived from a rigorous solution of Maxwell's equations (vector Helmholtz equations). Absorption integrals generalized for lossy one- and bi-periodic gratings and randomly rough 1D and 2D surfaces are expressed using conductivity tensors and the fields on the surface restricting a grating domain between uniform medias. Explicit formulae (in quadratures) for finding the absorption coefficients for one-periodic gratings working in conical diffraction and bi-periodic gratings and general 2D surfaces via diffraction problem parameters are presented using the normalization factors. Examples of absorption and scattering intensity problems calculated by the fast and accurate boundary integral equation method for one- and bi-periodic gratings and rough surfaces are demonstrated and compared with those calculated using the usual indirect and approximated approaches. An explicit computation of the absorption quantity A and the scattering intensity η is an important tool to check the quality of the numerical solution for absorbing and/or rough gratings and mirrors with the requirement that the sum of reflected, transmitted and total absorbed energies should be equal to the energy of the incident wave. Thus, the present energy balance approach for very general absorbing and/or scattering structures can be considered as universal and useful as the well known energy conservation laws for perfectly conducting and lossless gratings and rough mirrors. The direct and indirect results computed for the grating absorption and scattering coefficients are close for the presented numerical examples taken from various applications. Such a comparison is a good measure of accuracy of near-zone field calculus in a case when far-zone fields (intensities) are computed or measured accurately. Valuable differences between the scattering intensities of various surfaces show the need of using exact roughness statistics, diffraction and polarization angles, and rigorous methods in computations of practical significance for a sample.

Acknowledgements

The author thanks Gunther Schmidt for useful comments and Alexander Dashkov for numerical investigations.

Funding information

Funding for this research was provided by: Russian Science Foundation (grant No. 19-12-00270).

References

Ament, L., van Veenendaal, M., Devereaux, T., Hill, J. P. & van den Brink, J. (2011). *Rev. Mod. Phys.* **83**, 705–767.
Bakshi, V. (2018). Editor. *EUV Lithography*, 2nd ed. SPIE.
Bao, G. (1997). *SIAM J. Appl. Math.* **57**, 364–381.
Bao, G. & Dobson, D. C. (2000). *Proc. Am. Math. Soc.* **128**, 2715–2723.
Bao, G., Dobson, D. C. & Cox, J. A. (1995). *J. Opt. Soc. Am. A*, **12**, 1029–1042.
Boer, D. K. G. de (1996). *Phys. Rev. B*, **53**, 6048–6064.
Born, M. & Wolf, E. (2002). *Principles of Optics*, 7th exp. ed. Cambridge University Press.
Botten, L. C., Craig, M. S., McPhedran, R. C., Adams, J. L. & Andrewartha, J. R. (1981). *Opt. Acta: Int. J. Opt.* **28**, 1087–1102.
Botten, L. C., Nicorovici, N. P., Asatryan, A. A., McPhedran, R. C., de Sterke, C. M. & Robinson, P. A. (2000). *J. Opt. Soc. Am. A*, **17**, 2177–2190.
Budzinski, C., Güther, R. & Kleemann, B. (1991). *Optik*, **87**, 121–125.
Bugert, B. & Schmidt, G. (2015). *Discrete and Continuous Dynamical Systems – Series S*, **8**, 435–473.
Chkhalo, N. I. & Salashchenko, N. N. (2013). *AIP Adv.* **3**, 082130.
Choueikani, F., Lagarde, B., Delmotte, F., Krumrey, M., Bridou, F., Thomasset, M., Meltchakov, E. & Polack, F. (2014). *Opt. Lett.* **39**, 2141–2144.
CXRO (2020). *CXRO*, http://henke.lbl.gov/.
Dobson, D. C. (1994). *Model. Math. Anal. Numer.* **28**, 419–439.
Dobson, D. & Friedman, A. (1992). *J. Math. Anal. Appl.* **166**, 507–528.
Enoch, S. & Bonod, N. (2012). Editors. *Plasmonics From Basics to Advanced Topics*. Springer.
Goray, L. I. (2007). *J. Synch. Investig.* **1**, 362–367.
Goray, L. I. (2009). *Proc. SPIE*, **7390**, 73900V.
Goray, L. I. (2010*a*). *Waves Random Media*, **20**, 569–586.

Goray, L. I. (2010*b*). *J. Appl. Phys.* **108**, 033516.
Goray, L. I. (2013). *Proceedings of the International Conference Days on Diffraction 2013*, 27–31 May 2013, St Petersburg, Russia, pp. 65–71. IEEE.
Goray, L. I. (2015). *Proceedings of the International Conference Days on Diffraction 2015*, 25–29 May 2015, St Petersburg, Russia, pp. 123–129. IEEE.
Goray, L. I. (2016). *Proceedings of the International Conference Days on Diffraction 2016*, 27 June–1 July 2016, St Petersburg, Russia, pp. 177–181. IEEE.
Goray, L. I., Asadchikov, V. E., Roshchin, B. S., Volkov, Yu. O. & Tikhonov, A. M. (2019). *OSA Continuum*, **2**, 460–469.
Goray, L. I., Chkhalo, N. I. & Tsyrlin, G. E. (2009). *Tech. Phys.* **54**, 561–568.
Goray, L. I., Chkhalo, N. I. & Vainer, Yu. A. (2010). *Tech. Phys. Lett.* **36**, 108–111.
Goray, L. I. & Egorov, A. Yu. (2016). *Appl. Phys. Lett.* **109**, 103502.
Goray, L. I., Kuznetsov, I. G., Sadov, S. Yu. & Content, D. A. (2006*a*). *J. Opt. Soc. Am. A*, **23**, 155–165.
Goray, L., Jark, W. & Eichert, D. (2018). *J. Synchrotron Rad.* **25**, 1683–1693.
Goray, L. & Lubov, M. (2013). *J. Appl. Cryst.* **46**, 926–932.
Goray, L. & Lubov, M. (2015). *Opt. Express*, **23**, 10703–10713.
Goray, L. I., Pirogov, E., Sobolev, M., Ilkiv, I. V., Dashkov, A., Nikitina, E., Ubyivovk, E., Gerchikov, L. G., Ipatov, A., Vainer, Yu., Svechnikov, M., Yunin, P., Chkhalo, N. & Bouravlev, A. (2020). *J. Phys. D Appl. Phys.* **53**, 455103.
Goray, L. I. & Schmidt, G. (2010). *J. Opt. Soc. Am. A*, **27**, 585–597.
Goray, L. I. & Schmidt, G. (2012). *Phys. Rev. E*, **85**, 036701.
Goray, L. I., Seely, J. F. & Sadov, S. Yu. (2006*b*). *J. Appl. Phys.* **100**, 094901.
Hinode (2020). *Hinode*, http://hinode.nao.ac.jp/en/.
Huang, Q., Medvedev, V., van de Kruijs, R., Yakshin, A., Louis, E. & Bijkerk, F. (2017). *Appl. Phys. Rev.* **4**, 011104.
IIG (2020). *IIG*, http://pcgrate.com/.
IRMA (2014). *Nanotechnology: Concepts, Methodologies, Tools, and Applications.* Information Resources Management Association. Information Science Reference.
Jacobsen, C., Howells, M. & Warwick, T. (2019). *Springer Handbook of Microscopy*, edited by P. W. Hawkes & J. C. H. Spence, Springer Handbooks. Springer, Cham.
Jarem, J. M. & Banerjee, P. P. (1999). *J. Opt. Soc. Am. A*, **16**, 1097–1107.
Kozhevnikov, I. V. & Pyatakhin, M. V. (1998). *J. X-ray Sci. Technol.* **8**, 253–275.
Li, L. (2014). *J. Opt. Soc. Am. A*, **31**, 808–817.
Lingam, M. & Loeb, A. (2020). *ApJ*, **894**, 36.
Liu, Y. & Zhang, X. (2011). *Chem. Soc. Rev.* **40**, 2494–2507.
Loewen, E. G. & Popov, E. (1997). *Diffraction Gratings and Applications.* New York: Marcel Dekker.
Marlowe, H., McEntaffer, R. L., Tutt, J. H., DeRoo, C. T., Miles, D. M., Goray, L. I., Soltwisch, V., Scholze, F., Herrero, A. F. & Laubis, C. (2016). *Appl. Opt.* **55**, 5548–5553.
Marshall, H. L., Günther, H. M., Heilmann, R. K., Schulz, N. S., Egan, M., Hellickson, T., Heine, S. N. T., Windt, D. L., Gullikson, E. M., Ramsey, B., Tagliaferri, G. & Pareschi, G. (2018). *J. Astron. Telesc. Instrum. Syst.* **4**, 011005.
Maystre, D. & Saillard, M. (1994). *Waves in Random Media*, **4**, 467–485.
Nau, D., Schönhardt, A., Bauer, Ch., Christ, A., Zentgraf, T., Kuhl, J., Klein, M. W. & Giessen, H. (2007). *Phys. Rev. Lett.* **98**, 133902.
Nieto-Vesperinas, M. & Dainty, J. C. (1990). *Scattering in Volumes and Surfaces.* Amsterdam: North-Holland.
Ogilvy, J. A. (1987). *Rep. Prog. Phys.* **50**, 1553–1608.
Petit, R. (1980). Editor. *Electromagnetic Theory of Gratings.* Berlin: Springer.
Popov, E. (2014). Editor. *Gratings: Theory and Numerical Applications*, 2nd rev. ed. Presses Universitaires de Provence, AMU.
Rathsfeld, A., Schmidt, G. & Kleemann, B. H. (2006). *Commun. Comput. Phys.* **1**, 984–1009.
Roger, A., Vincent, P., Nevière, M. & Reinisch, R. (1984). *Phys. Rev. B*, **29**, 5570–5574.
Sadiku, M. N. O. (2009). *Monte Carlo Methods for Electromagnetics.* CRC Press, Taylor & Francis Group.
Saillard, M. & Maystre, D. (1988). *J. Opt.* **19**, 173–176.
Saillard, M., Maystre, D. & Rossi, J. P. (1986). *J. Mod. Opt.* **33**, 1193–1206.
Saillard, M. & Sentenac, A. (2001). *Waves Random Media*, **11**, R103–R137.
Schmidt, G. (2003). *Appl. Anal.* **82**, 75–92.
Seely, J., Kjornrattanawanich, B., Goray, L., Feng, Y. & Bremer, J. (2011). *Appl. Opt.* **50**, 3015–3020.
Shatokhin, A. N., Kolesnikov, A. O., Sasorov, P. V., Vishnyakov, E. A. & Ragozin, E. N. (2018). *Opt. Express*, **26**, 19009–19019.
Siewert, F., Löchel, B., Buchheim, J., Eggenstein, F., Firsov, A., Gwalt, G., Kutz, O., Lemke, S., Nelles, B., Rudolph, I., Schäfers, F., Seliger, T., Senf, F., Sokolov, A., Waberski, C., Wolf, J., Zeschke, T., Zizak, I., Follath, R., Arnold, T., Frost, F., Pietag, F. & Erko, A. (2018). *J. Synchrotron Rad.* **25**, 91–99.
Sinha, S. K., Sirota, E. B., Garoff, S. & Stanley, H. B. (1988). *Phys. Rev. B*, **38**, 2297–2311.
Sisodia, M. L. & Gupta, V. L. (2007). *Microwaves: Introduction to Circuits, Devices and Antennas.* New Age International.
Smith, B. W. & Suzuki, K. (2007). Editors. *Microlithography: Science and Technology*, 2nd ed. CRC Press.
Stearns, D. G. (1992). *J. Appl. Phys.* **71**, 4286–4298.
Stockman, M. I., Faleev, S. V. & Bergman, D. J. (2001). *Phys. Rev. Lett.* **87**, 167401.
Strocov, V. N., Schmitt, T., Flechsig, U., Schmidt, T., Imhof, A., Chen, Q., Raabe, J., Betemps, R., Zimoch, D., Krempasky, J., Wang, X., Grioni, M., Piazzalunga, A. & Patthey, L. (2010). *J. Synchrotron Rad.* **17**, 631–643.
Stuart, H. R. & Hall, D. G. (1998). *Phys. Rev. Lett.* **80**, 5663–5666.
Tsang, L., Kong, J. A., Ding, K.-H. & Ao, C. O. (2001). *Scattering of Electromagnetic Waves: Numerical Simulations.* New York: Wiley.
Vannoni, M. & Freijo-Martin, I. (2017). *Opt. Express*, **25**, 26519–26526.
Voronov, D. L., Goray, L. I., Warwick, T., Yashchuk, V. V. & Padmore, H. A. (2015). *Opt. Express*, **23**, 4771–4790.
Voronov, D. L., Salmassi, F., Meyer-Ilse, J., Gullikson, E. M. T., Warwick, T. & Padmore, H. A. (2016). *Opt. Express*, **24**, 11334–11344.
Warnick, K. F. & Chew, W. C. (2001). *Waves Random Media*, **11**, R1–R30.
Weitz, D. A., Gramila, T. J., Genack, A. Z. & Gersten, J. I. (1980). *Phys. Rev. Lett.* **45**, 355–358.
Yashchuk, V. V., Samoylova, L. V. & Kozhevnikov, I. V. (2015). *Opt. Eng.* **54**, 025108.